Relative Roles of Large-Scale Orography and Land Surface Processes in the Global Hydroclimate. Part I: Impacts on Monsoon Systems and the Tropics

TETSUZO YASUNARI

Frontier Research Center for Global Change, Japan Agency for Marine-Earth Science and Technology, Yokohama, Kanagawa, and Hydrospheric Atmospheric Research Center, Nagoya University, Nagoya, Aichi, Japan

KAZUYUKI SAITO AND KUMIKO TAKATA

Frontier Research Center for Global Change, Japan Agency for Marine-Earth Science and Technology, Yokohama, Kanagawa, Japan

(Manuscript received 12 May 2005, in final form 5 January 2006)

ABSTRACT

A series of numerical simulations by an atmospheric general circulation model (AGCM) was conducted to evaluate the relative roles of Tibetan Plateau (TP) and continental-scale land surface processes on the Asian monsoon and hydroclimates in other regions in the Tropics. Four boundary conditions were used to define experiments: a flat and bare-rock (nonvegetated) surface (NMR), a realistic TP with bare-rock surface (MR), MR conditions but with a water-holding soil layer (with 20 cm of field capacity) (MS), and TP with a vegetated surface with specified albedo and roughness of the current vegetation and the soil layer (MVS).

Systematic increases of precipitation (P) over the Asian monsoon region and other land areas in the Tropics were noticed from NMR, MR, MS, to MVS runs. Precipitation over the warm tropical western Pacific, in contrast, decreased from NMR to MVS runs although the same SST climatology was prescribed in all the experiments. The effect of TP orography produces wet (dry) climate regions to the west (east) of TP as shown in other GCM studies. In the Asian monsoon region both land surface effect (LSE) and TP effect (TE) contribute nearly equally to increase P, but in the West African monsoon region, TE contributes to decrease P while LSE plays a major role to increase P. LSE also enhances the subtropical anticyclone over the North Pacific through enhanced land–ocean thermal contrast.

In most of the monsoon regions and Tropics, the albedo (and roughness) effect of vegetation substantially increases available radiation, which in turn increases both evaporation (E) and atmospheric moisture convergence (C), and, as a result, significantly increases P. This positive feedback between E and C is likely to be a characteristic nature when and where vegetation albedo effect is significant under sufficient radiative energy, suggesting a prerequisite for Charney's original hypothesis.

1. Introduction

Monsoons are large-scale circulation systems induced by seasonal differential heating between land and oceans. Variabilities in monsoon systems can therefore be attributed to changing characteristics in energy storage and transfer processes between land, atmosphere, and oceans. Many previous studies have examined the influence of oceans on monsoon systems, focusing particularly on the impact of sea surface temperature (SST) changes, including El Niño–Southern Oscillation (ENSO), regulating large-scale circulation and moisture supplies relevant to the monsoon system.

This study explored how various land surface processes impact the monsoon systems through modulation of land–ocean heating contrast. Many previous modeling studies have considered the effect of large-scale orographies (e.g., the Tibet–Himalayan mountains) (e.g., Manabe and Terpstra 1974; Hahn and Manabe 1975; Nigam et al. 1986, 1988; Broccoli and Manabe 1992) by removing or changing them. Some recent studies using coupled ocean–atmosphere general circulation models (GCMs) have also suggested that changes in the Tibetan Plateau greatly impact the Asian monsoon system and the atmosphere–ocean coupled

Corresponding author address: Tetsuzo Yasunari, Frontier Research Center for Global Change, JAMSTEC, Yokohama, Kanagawa 236-0001, Japan.
E-mail: yasunari@hyarc.nagoya-u.ac.jp

system in the equatorial Pacific (Abe et al. 2003, 2004; Kitoh 2002). Surface vegetation and soil conditions, such as prescribed albedo and field capacity, were constant in these studies.

Other studies that used prescribed orography have considered the effect of vegetation by varying parameters related to vegetation (e.g., albedo, roughness parameters, stomatal conductance) (Sato et al. 1989; Xue et al. 2004). These studies showed that changing surface vegetation conditions also strongly influence the intensity and time–space structure of the Asian monsoon. Recent studies have further examined how changing soil moisture conditions, which are determined by prescribing realistic soil moisture conditions or by changing soil layer characteristics such as the water-holding field capacity (Manabe et al. 1965) of the surface soil layer affect rainfall in the monsoon region (e.g., Milly and Dunne 1994; Dirmeyer and Shukla 1996; Kanae et al. 2006).

However, no attempt has yet been made to evaluate the relative importance or role of both large-scale orography and land surface processes (including soil, vegetation skin, and subgrid-scale biophysics) on the formation of the monsoon or on the hydroclimate over the continent and surrounding oceans. Soil and vegetation conditions, in reality, constitute a combined land surface system; the soil layer has formed through interactions with vegetation (Jenny 1941) as well as through physical and chemical processes such as weathering. The consideration of relative roles of these two major land processes/conditions (dynamical effects of large-scale orography and physical effects of vegetation) may also be instrumental for assessing the role of continents in the evolution of a climate system in the long history of the earth.

To deduce the effects of different land surface conditions on the monsoon climate system, a simulation with a "bare rock" surface, representing the nonvegetated "original continent," should first occur. That simulation can be followed by simulations that separately consider three effects: orography, soil under the surface, and a vegetated surface. These three factors that control land surface conditions represent the basic stages in the evolution of continental soil and surface during the earth's climatic history. Simulations that include present realistic continental surfaces are an integration of all these factors (Buol et al. 1997). Comparisons of results from different numerical settings can provide quantitative and qualitative estimates of the essential and key role of land as part of the fundamental processes in the real climate system. At this stage of the research, we decided to use a medium horizontal resolution (ca. 2.85° gridding) and a simple land surface scheme with bucket-type hydrology with simple bulk stomatal resistance, and with vegetation albedo and roughness. This simple setting may partly distort the model outputs due to a lack of detailed vegetation biophysical processes and to a coarse resolution. Nonetheless, we consider that the result of this preliminary study is useful to draw a simplistic picture of the basic mechanisms on atmospheric energy process and hydrological cycle over land, derived from the same configuration in the land surface scheme with different values of relevant parameters (e.g., surface albedo, field capacity, and altitude), and from relatively long integration (50 yr). With this framework, relative effects of orography, soil, and vegetation skin (by specified vegetation albedo and roughness) are investigated, in contrast to Xue et al. (2004) where biophysical effects were studied. The first part of this paper focuses on the monsoon system through modulation of heating contrast between land and ocean. The second part discusses seasonal climatology and hydroclimate evolution over Eurasia (Saito et al. 2006, hereafter Part II).

This study discusses results from a series of numerical experiments using an atmospheric GCM. The experimental design is based on the speculation on large-scale land surface conditions stated above, and is described in the next section. Section 3 describes the results, focusing on global or hemispheric atmospheric changes; section 4 details regional aspects of hydroclimate changes over some monsoon regions and the Tropics. A discussion and conclusions follow in section 5.

2. Model and experimental design

The model used in this study is version 5.7b of the Center for Climate System Research/National Institute for Environmental Studies/Frontier Research Center for Global Change atmospheric general circulation model (CCSR/NIES/FRCGC AGCM). The model is a three-dimensional hydrostatic primitive equation (Haltiner and Williams 1980) model in spherical sigma coordinates. Overall features and performance of the atmospheric part of the model are described in Numaguti (1999). The model included triangular truncation of up to 42 wavenumbers (T42 horizontal resolution); this truncation is equivalent to a horizontal grid size of ca. 2.5° in longitude and latitude. The vertical axis is a sigma coordinate and has 20 levels, up to about 10 hPa in the lower stratosphere; vertical discretization follows Arakawa and Suarez (1983). A semi-implicit leapfrog time integration is used. Ocean surface conditions (sea surface temperatures and sea ice condensation) are pre-

scribed by monthly climatology for 1979–1989 adopted from the Atmospheric Model Intercomparison Project (AMIP) (Gates 1992).

Radiation in the model is parameterized using the two-stream k-distribution scheme (Nakajima et al. 2000). Cumulus parameterization is a simplified Arakawa–Schubert scheme (Arakawa and Schubert 1974; Moorthi and Suarez 1992). Large-scale condensation prognostic cloud water is parameterized as in Le Treut and Li (1991). The second-order Mellor–Yamada level-2 closure scheme (Mellor and Yamada 1974) with simple cloud effects parameterizes vertical diffusion by turbulence. Orographic gravity wave drag is parameterized following McFarlane (1987).

The land surface scheme used in this study is based on bucket-type hydrology as stated in the introduction. The explicitly controlled factors of the "surface vegetation" processes are vegetation albedo and roughness. The scheme, however, does not include subgrid-scale, biophysical parameterizations in comparison with "vegetation" models such as the Simple Biosphere Model (SiB2; Sellers et al. 1996), and therefore the assessment made in this study should be considered as preliminary. Vegetation types and albedo values (invariant with seasons) are adopted from Matthews (1983). The roughness is specified for each surface vegetation type after Kondo (1994) and is modified in accordance with snow amount. The fixed values for daytime and nighttime conditions are assigned to stomatal resistance.

The land surface scheme has one hydrological layer of 1-m depth and three thermal layers to the depth of 2 m (Numaguti 1999). The water-holding capacity (saturation soil water storage) of the soil is parameterized by a predefined value of field capacity (FC). The ground wetness is prognostically determined by the balance of precipitation, evapotranspiration, snowmelt, and runoff. Water in the soil layer that exceeds the FC is removed from the system as runoff. The heat conduction equation determines prognostically the ground temperature profile so that it reproduces diurnal and seasonal variations. Vertical turbulent fluxes at the surface are estimated by bulk formulas. Aerodynamic resistance is diagnostically determined. The evaporation efficiency is estimated from soil wetness, aerodynamic resistance, and stomatal resistance (specified as in the previous paragraph), so that latent heat flux indirectly includes the effect of transpiration.

Four simulations with different surface boundary conditions were considered in this study. The bare-rock land surface was considered as a nonvegetated surface, and therefore the effects of soil/vegetation were divided into two parts: above the surface and below the surface. Factors above the surface include albedo and roughness length (Z_0). A vegetated surface generally has a lower surface albedo that affects incoming radiation at the surface. Similarly, roughness length directly affects fluxes of momentum, heat, and water vapor between the boundary layer and the free atmosphere. Factors below the surface include water-holding capacity (or FC), which represents the most essential function of vegetation and soil below the surface. The FC directly controls hydrological flux and indirectly controls heat flux across the surface through apparent heat capacity. Last, surface altitude was included to gauge the effect of orography.

The first experiment was the run with bare-rock flat surface of the Eurasian continent, by removing the large-scale orography east of 30°E over Eurasia including the Arabian Peninsula and the Tibetan Plateau. To mimic bare-rock (i.e., nonvegetated) conditions, FC was set to 0.01 m, and surface albedo was set to desert condition (=0.3). This was the NMR run. The second experiment was the same as the first experiment but with the orography over the Eurasian continent (MR run). Differences between the MR and NMR runs suggest marginal effects linked to the presence of large-scale orography over eastern Eurasia where the land surface shows desert conditions. The third experiment was the run with the same conditions as those of the MR run except the soil surface condition (with FC = 0.2 m). This was MS run. Differences between the MS and MR runs suggest effects related to soil-layer surfaces.

The fourth experiment (MVS run) was the run with the same conditions as those of the MS run, except the vegetated surface conditions. Albedo and roughness length at each grid point are given values that correspond to the prescribed realistic vegetation type at the grid point. Albedo varied from 0.11 to 0.28, and roughness length varied from 0.003 to 2.0 m for different vegetation types. At all land grid points FC was set to 0.2 m. This run was, therefore, closest to the reality in terms of surface boundary conditions.

Figure 1 shows experimental designs for the NMR, MR, MS, and MVS runs, and Table 1 summarizes the parameter values of each experiment. Figure 2 shows spatial distribution of albedo and orography for the two typical cases, that is, (a) MVS run and (b) NMR runs. The models in each of the four experiments were integrated for 50 yr following a 5-yr spinup. Monthly or seasonal "mean climate" values were computed as averages of the last 40 yr; pentad "mean climate" values represent averages of the last 25 yr. Mean climates for each experiment were used to deduce the impacts of land surface conditions.

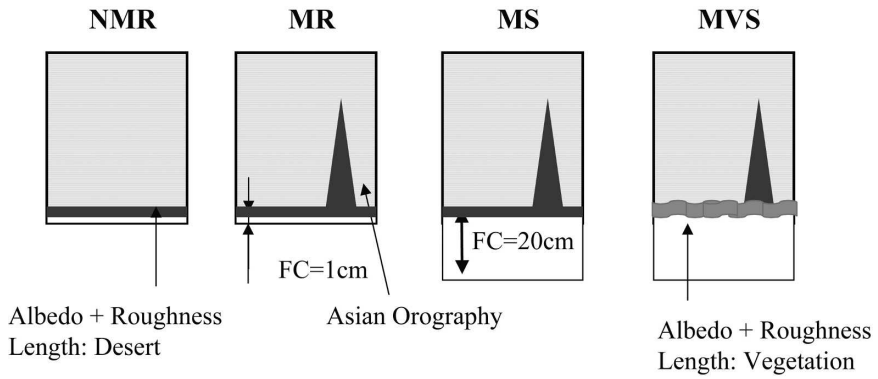

FIG. 1. Schematic illustration of vegetation, soil, and Asian orography for four experimental settings.

3. Changes in the planetary-scale monsoon system

Changes in land surface conditions affect planetary-scale monsoon systems during the Northern Hemisphere summer. Figure 3 shows precipitation for (a) NMR, (b) MR, (c) MVS, and (d) the observation taken from the Climate Prediction Center (CPC) Merged Analysis of Precipitation (CMAP) data (Xie and Arkin 1997). Figure 4 shows the difference map of June–August (JJA) precipitation and wind field at 850 hPa for (a) MR minus NMR and (b) MVS minus MR. The zone of precipitation between 10° and 15°N was considered an intertropical convergence zone (ITCZ) in NMR (Fig. 3a). In this ITCZ, more precipitation (>400 mm month^{-1}) fell over oceans than over land. Heaviest amounts fell over the Pacific, with somewhat lighter amounts occurring over the South China Sea and the Bay of Bengal in the Asian monsoon region. Precipitation was light (less than 100 mm month^{-1}) over most of the continent. When there is no Tibetan Plateau (TP), no vegetated surface with high albedo, and near-zero FC over land, overall monsoon effects are very weak (Fig. 3a). The MR run (Fig. 3b) included a TP but no vegetated surface. Precipitation in this simulation increased over the Bay of Bengal and a zone of light precipitation (around 200 mm month^{-1}) appeared over land, centered south and southeast of the TP as shown in Fig. 4a. Orographic effects of the TP are important in the formation of the Asian summer monsoon. Note, however, that precipitation amounts particularly over land in this MR simulation were lighter than observed values. The MVS run (Fig. 3c) showed that heaviest precipitation appears over the Bay of Bengal, but the ITCZ over the Pacific Ocean was drastically weakened. A broad area of south, southeast, and east Asia received heavy precipitation (exceeding 300 mm month^{-1}). This distribution over land is very similar to that observed in the summer monsoon season (Fig. 3d).

TABLE 1. Summary of the land surface conditions in the simulations.

	Vegetation type at grids	Albedo	Roughness (m)	Field capacity (m m^{-1})	Asian mountains
MVS	Specified	0.11–0.28	0.003–2.0	0.2	With
MS	Desert	0.3	0.02	0.2	With
MR	Desert	0.3	0.02	0.01	With
NMR	Desert	0.3	0.02	0.01	Without

Figure 5 shows global streamfunction and wind field except south of 30°S in the lower troposphere (850 hPa) for the three runs (NMR, MR, and MVS). The difference fields of these parameters between MR and NMR and between MVS and MR are also shown in Fig. 6. In the NMR run (Fig. 5a) although cross-equatorial flow and monsoon-like westerly flow is dominated over the northern tropical Indian Ocean, a center of convergence associated with precipitation maximum (see Fig. 3a) is located over the western Pacific. A cyclonic circulation corresponding to the monsoon trough over the Indian subcontinent through the Indo-China Peninsula is so broad and no southwesterly appears over southeast Asia and China. In the MR run (Fig. 5b) the southwesterly monsoon flow is now dominated over the Arabian Sea, and southwesterly appears over the Indo-China and to the southeast of TP, and the southerly component, though weak, appears over China. The difference field between MR and NMR (Fig. 6a) clearly demonstrates anomalous anticyclonic circulation over northeastern Eurasia, which is formed primarily through deflection of midlatitude westerly flow by the large-scale orography over there. Another remarkable change between MR and NMR is the appearance of cyclonic circulation to the west of TP as clearly shown

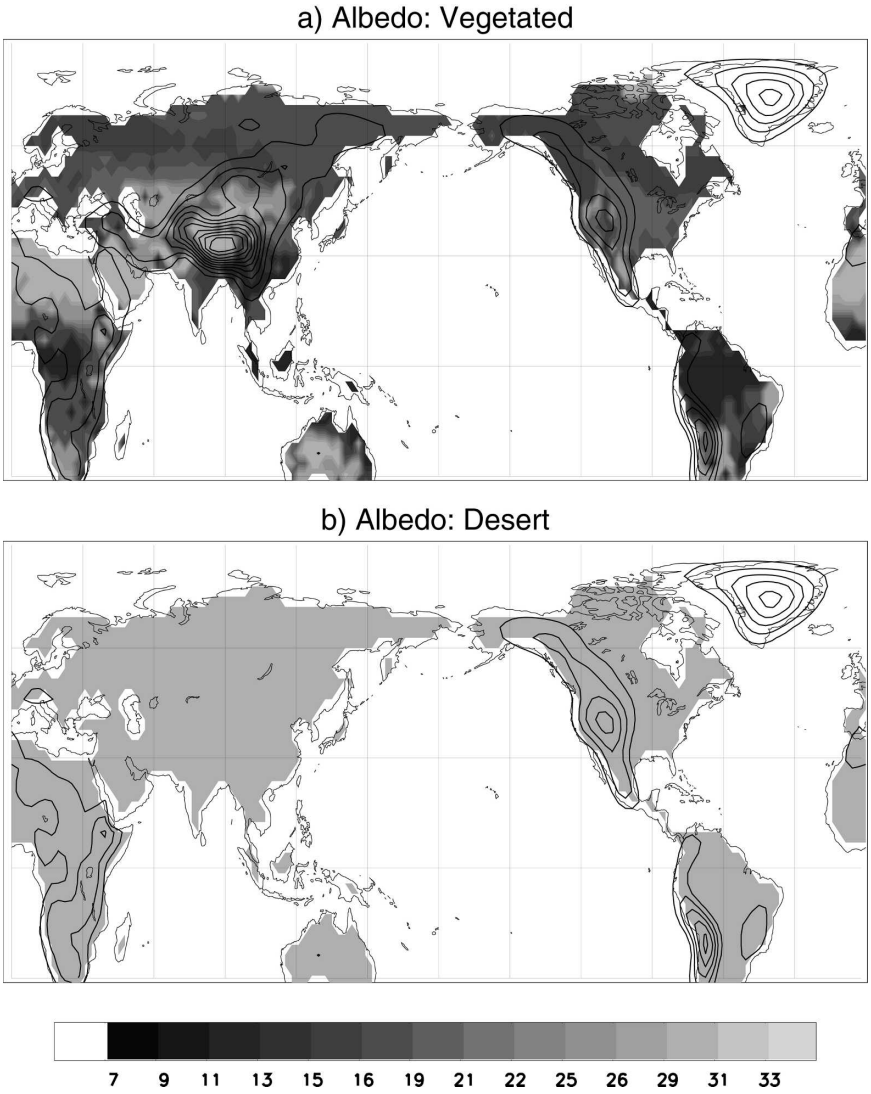

FIG. 2. (a) Albedo maps for vegetated land surfaces (shades) and the Asian orography including Tibetan Plateau (contours) used for MVS run. Contour interval is 500 m. (b) As in (a), but for a desert land surface without the Asian orography used for NMR run.

in Fig. 6a. This may be due to a stationary Rossby wave response to dynamical and thermodynamical effect of TP as Rodwell and Hoskins (1996) discussed. In the MVS run (Fig. 5c) the overall feature as shown in Fig. 5b is further intensified. Southwesterly monsoon flow is now dominated to the southeast of TP and east Asia, and westerly flow over the western Pacific is weakened. Of particular interest may be a further intensification of the subtropical high over the North Pacific, as is clearly shown in the difference field between MVS and MR (Fig. 6b). This may be closely related to the intensification of surface and atmospheric heating (as suggested in Fig. 4b, and as shown in Fig. 3 of Part II) over the vegetated Eurasian continent, presumably through the Rossby wave response originating to the west of the monsoon heating (Rodwell and Hoskins 2001).

Figure 7 shows global streamfunction, except south of 30°S, in the upper troposphere (200 hPa) for the three runs. In the NMR run (Fig. 7a), a subtropical anticyclone dominated over the western Pacific, a region that corresponded to the center of convection and heating (Fig. 4a). A minor anticyclone also developed over Mexico. In the MR run (Fig. 7b), features over and around Asia were dramatically different from those in the NMR run. A very large subtropical anticyclone formed over the subtropics of Eurasia, centered over the TP. This anticyclone corresponds to the "Tibetan high" in the present climate system. The difference

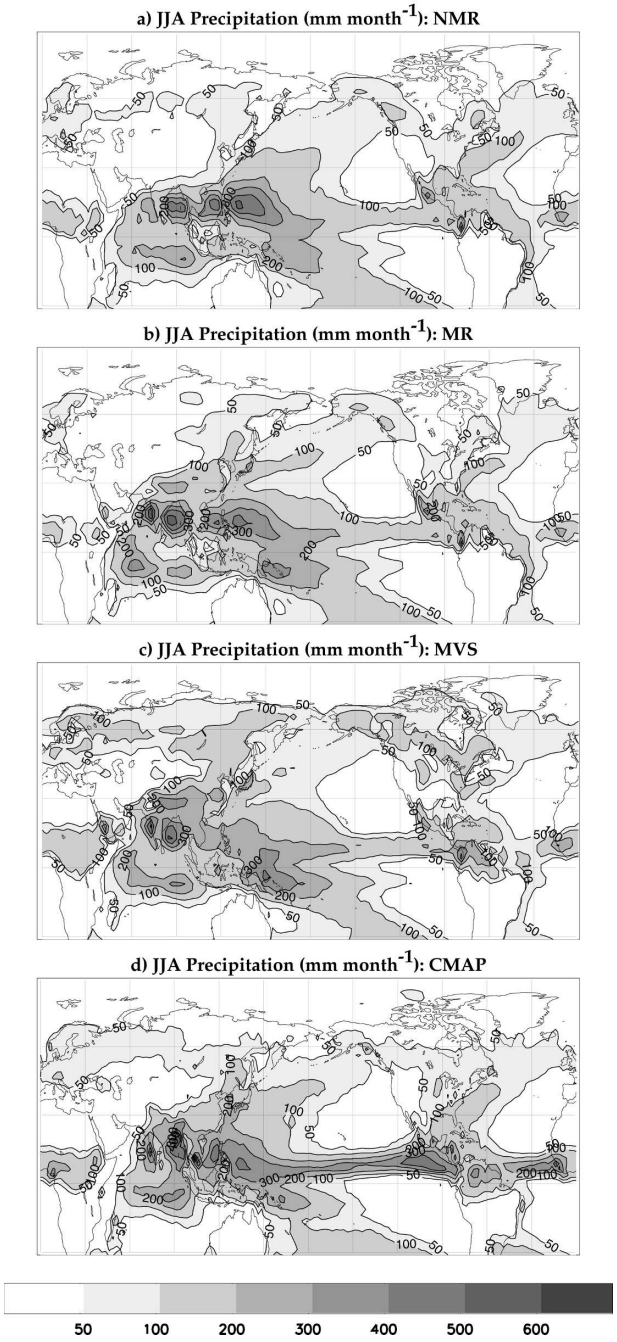

FIG. 3. Map of precipitation (contours) and wind at 850 hPa (arrows) for (a) NMR, (b) MR, and (c) MVS runs, and (d) observation from CMAP for JJA. The contour interval is 50 mm month^{-1}.

field (Fig. 8a) shows enhancement of anticyclonic circulation to the west TP, suggesting that dynamical and thermodynamical effect of TP enhances the Tibetan high through the stationary Rossby wave response (Rodwell and Hoskins 1996).

The anticyclonic circulation over North America was also stronger in MR than in NMR even though orographic changes occurred only over Eurasia (mainly TP). Tibetan Plateau orography may force a planetary-scale stationary wave that also intensifies the anticyclonic circulation over the Mexican highlands. This effect is also shown in the difference field between MR and NMR in Fig. 8a.

In the MVS run (Fig. 7c), a broader Tibetan anticyclone over Asia and deeper trough over the central North Pacific further enhanced the overall circulation pattern. Difference fields between MVS and MR runs (Fig. 8b) show overall northward shift of the upper anticyclonic circulation particularly over the eastern Eurasia, showing further enhancement of the planetary-scale monsoon circulation.

4. Changes in regional-scale hydroclimates and surface budgets

a. Changes in regional-scale surface energy budgets

Regional energy and water budgets change as orography and land surface conditions (i.e., NMR, MR, MS, and MVS) change. This study focused on changes over six land areas in the Asian monsoon region and other tropical regions shown in Fig. 9: south/Southeast Asia (SA), east Asia (EA), West Africa (WA), the Indonesian Maritime Continent (MC), Amazonia (Am), and Siberia (Sb).

Table 2 shows that the overall effect of vegetation albedo and roughness on the energy budget (as inferred from changes from MR to MS, MS to MVS) is to reduce sensible heating (H) and increase latent heating (LE). In south/Southeast Asia and east Asia, the ratios of LE to net radiation (R), LE/R, increase from NMR to MR due to moisture supply increase by invasion of monsoon flow. No significant changes appear in MC and in Sb. The increase of FC from MR to MS dramatically increases LE/R in all the regions through increase of evaporation efficiency. In the monsoon regions increase of FC seems to be more effective in EA (LE/R increases from 0.58 to 0.82) than in SA (LE/R increases from 0.77 to 0.89) in forcing evaporation because of more effective soil moisture memory under relatively dry conditions. From MS to MVS increases of R are common in all the regions, though the ratios LE/R do not change significantly. The overall effects of vegetation albedo and roughness (as inferred from the changes of LE and LE/R from MR to MVS) are significant particularly in the tropical rain forest regions (MC and Am), and in mid-/high latitudes of Asia (EA and Sb), where the increasing rate of LE and LE/R range from 180% to 230%. The rate in the tropical monsoon regions (SA and WA) is relatively small

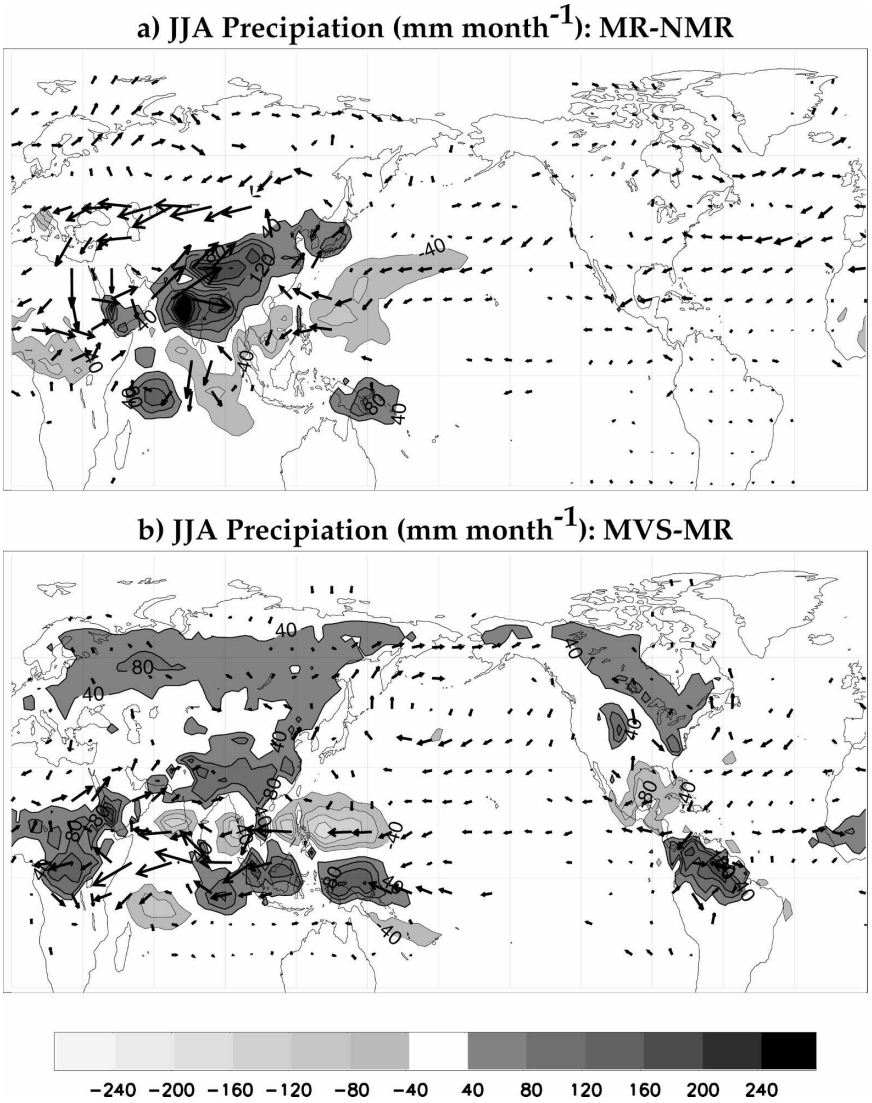

FIG. 4. (a) Difference map of JJA precipitation (contours) and 850-hPa wind (arrows) between (a) MR and NMR and (b) MVS and MR. The contour interval is 40 mm month^{-1}. Zero contours are suppressed. Only wind differences with speeds exceeding 1 m s^{-1} are shown.

(around 130%), since the original LE values are already high in MR.

b. Changes in regional-scale water budgets

Figure 10 shows changes in the seasonal course of precipitation in each area. The observed precipitation climatology is also shown in each region, adopted from CMAP. Table 3 shows changes in atmospheric water budgets, during the same seasons as in Table 2.

The overall features of MVS precipitation in the tropical monsoon regions (SA and WA) very well match the present precipitation climatology both in quantities and in seasonal patterns. Seasonal march of EA in MVS is also similar to that observed, though the amount in rainy season is overestimated to a small extent by about 20%. We may assume, therefore, the MVS corresponds to the most realistic simulation of the current Asian monsoon system. Precipitation in NMR in the Asian monsoon regions (SA and EA) shows about a half or less of that in MVS. This suggests that a land–ocean heating contrast without TP and land surface processes explain only a half or less of the precipitation in the realistic Asian monsoon system. Once TP topography is introduced, precipitation over these monsoon regions increased to about two-thirds of that in MVS (as referred from differences between MVS

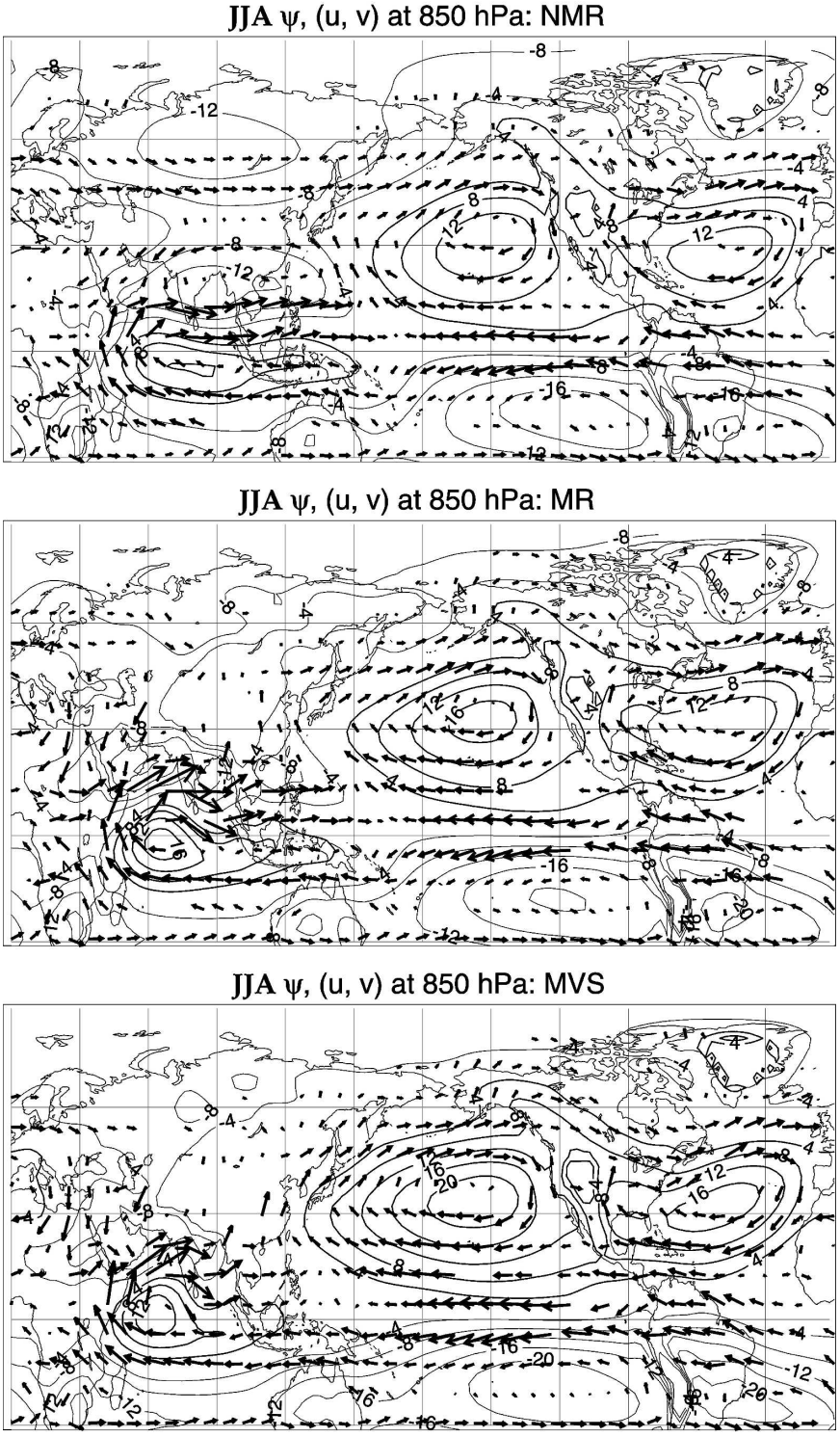

FIG. 5. JJA streamfunction and wind at 850 hPa for (a) NMR, (b) MR, and (c) MVS. Contours are every 10×10^6 m^2 s^{-1}.

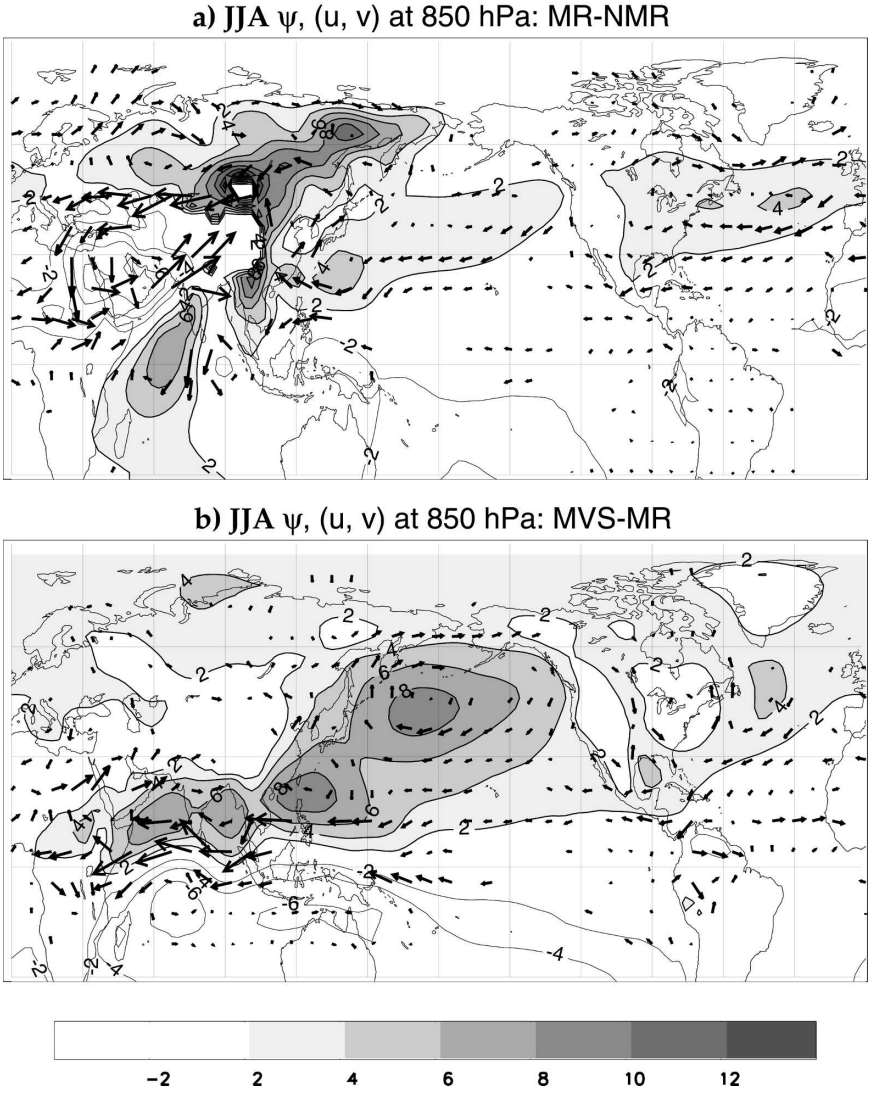

FIG. 6. As in Fig. 5 but for streamfunction and wind at 850 hPa. Contours are every 2×10^6 $m^2 s^{-1}$. Zero contours are suppressed. Only wind differences with speeds exceeding 1 $m s^{-1}$ are shown.

and MR). Atmospheric heating over and around TP plays an essential role in producing the monsoon flow, by enhancing cyclonic circulation (monsoon trough) as shown in Fig. 6a.

A distinct difference between SA and EA arises in comparisons of MR, MS, and MVS runs. As is also discussed in section 4a, in EA the increase of FC increases E more effectively (as inferred from the difference between MS and MR) compared to SA. That is, the amount of E in EA is comparable to that in SA for the MS and MVS run, but it is only two-thirds of that for the MR run. The ratio of E to convergence (C), E/C, for the MVS run exceeds 2 over EA, but it is only 1.1 over SA. Thus, the soil/vegetation layer over EA is more likely to increase precipitation efficiently by enhancing E from the wet soil/vegetation layer.

On the other hand, the change from MR to MS condition (i.e., increase of FC) may induce a negative feedback between E and C over EA, while a positive feedback tends to occur over SA. This positive feedback between E and C may be a characteristic nature of humid Tropics where increase of E could enhance large-scale convection, which, in turn, enhances convergence (Dirmeyer and Shukla 1996; Zeng 1998).

Differences of precipitation over WA between the four runs differ considerably from differences in the Asian monsoon regions. Interestingly, precipitation in MR (with TP) is lighter than that in NMR (without TP).

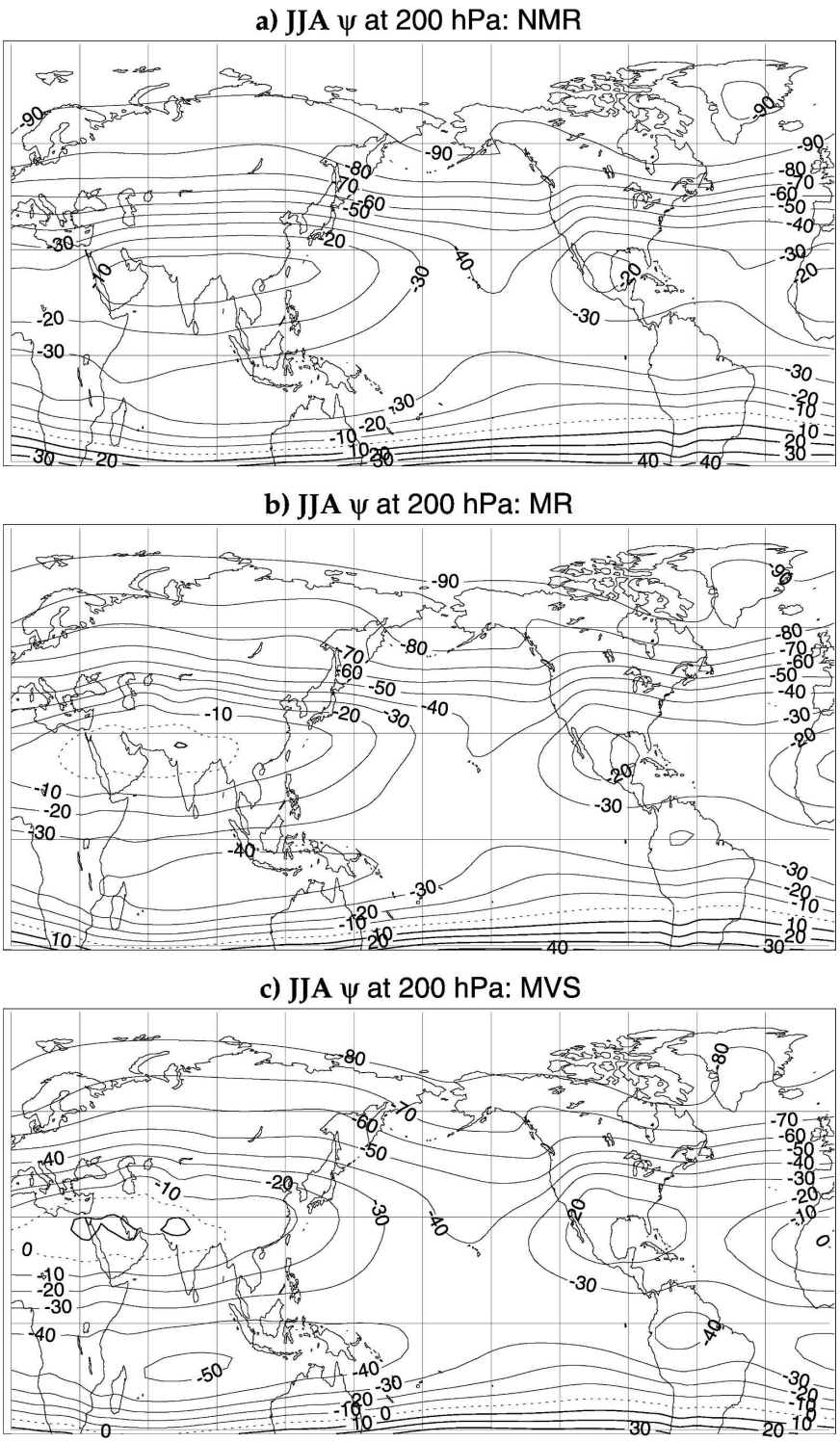

FIG. 7. JJA streamfunction at 200 hPa for (a) NMR, (b) MR, and (c) MVS. Contours are every 10×10^6 m^2 s^{-1}.

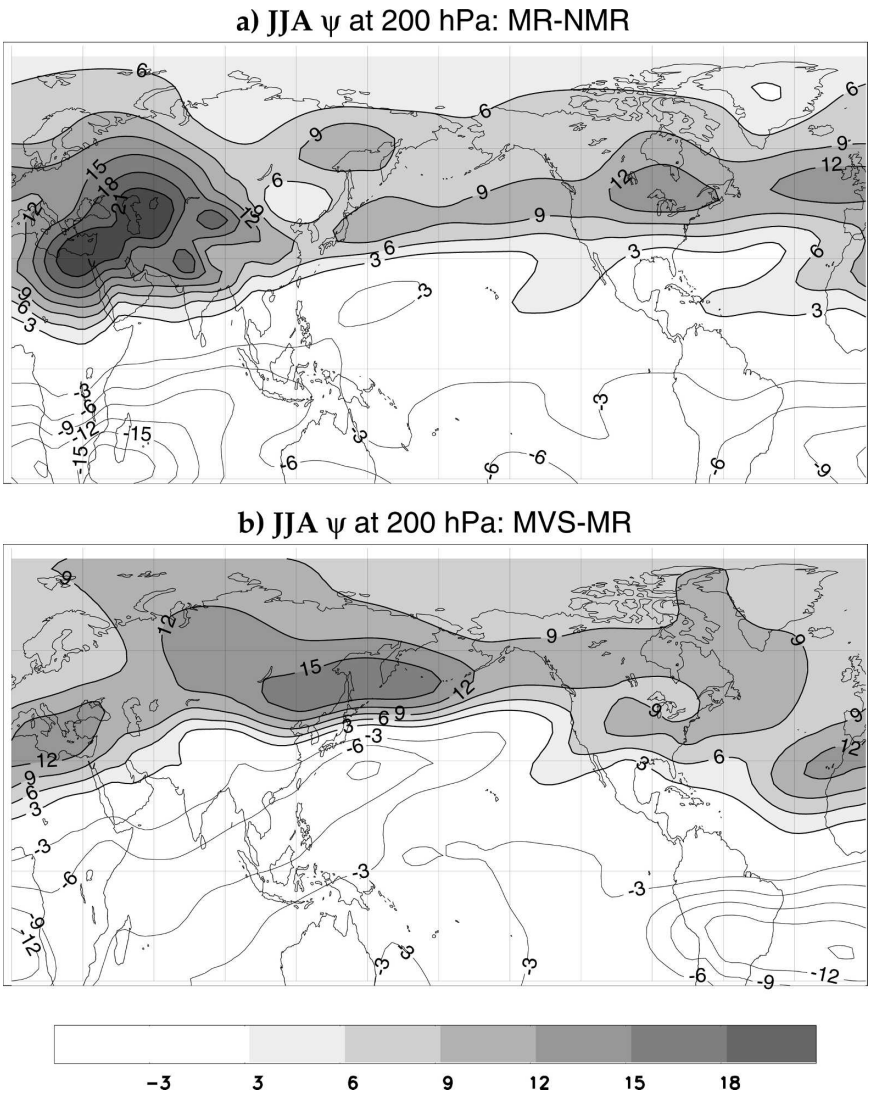

FIG. 8. As in Fig. 7 but for 200 hPa. Contours are every 3×10^6 m^2 s^{-1}.

The TP orography plays an essential role in enhancing downward motion and dry climate conditions over western Africa. The cause is likely an enhanced east–west circulation between Asia and Africa, and interaction with the stationary Rossby wave to the west of monsoon heating, as suggested in previous modeling studies (e.g., Manabe and Terpstra 1974; Rodwell and Hoskins 1996).

Over MC, the effect of TP orography seems to be negligible (from the difference between NMR and MR shown in Fig. 10d), and a systematic increase of precipitation from MR, MS, to MVS is noticeable, mainly due to increase of E (Table 3). The land surface effect (FC, vegetation albedo, and roughness) included in the MVS run suggests the positive feedback between E and C, similar to the other tropical regions. However, all four runs have failed to simulate observed seasonal cycle with a maximum precipitation in northern winter. This systematic error may, at least partly, be related to lack of spatial resolution in the complex geography of this region that winter monsoon rainfall over this region cannot be fully reproduced in the relatively coarse model resolution. Over Am in the equatorial South America, the overall changes of precipitation from MR, MS, to MVS (Fig. 10e) are similar to those over MC, indicating the dominant role of vegetation in increasing precipitation. The MVS run well simulated precipitation with its seasonal cycle except early for summer months (November and December).

Changes in precipitation, energy, and water balances over Sb are also shown in Fig. 10f and Tables 2 and 3, respectively, to compare with hydroclimate responses

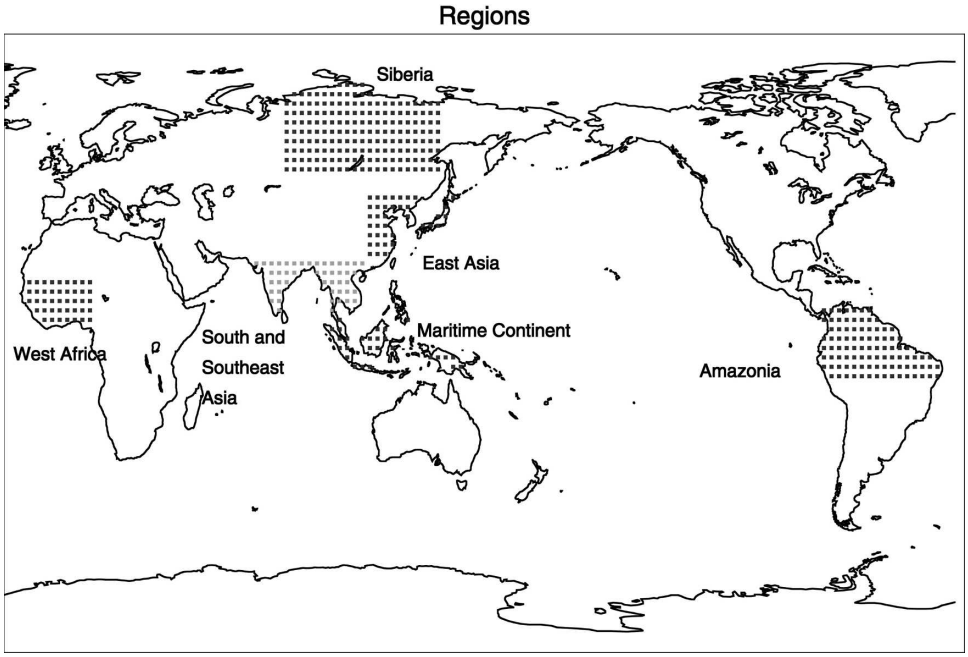

FIG. 9. Definition of six land areas used for analysis.

in the Tropics. The seasonal cycle is too much enhanced, particularly with a large maximum precipitation in northern summer when the TP orography is introduced. In addition, summer precipitation increases dramatically when vegetation albedo and roughness are introduced (MS and MVS runs). In midsummer (July to August) the FC effect is important for increasing precipitation (because of enhanced evaporation). In spring to early summer (March to June), albedo effects are most important, presumably due to soil moisture supplied by increased snowmelt. However, caution may be needed to discuss the large precipitation and evaporation in summer, because these seem to be extremely large compared to the observations as shown in Fig. 10f. These systematic biases in summer water balance may be, at least partly, related to the exclusion of some important effect of vegetation (e.g., full stomatal resistance and/or leaf area index) in the land surface processes. Sato et al. (1989) and Xue et al. (2004) showed, for example, that evapotranspiration and associated precipitation over the forested area in northern continents were considerably suppressed by adopting the SiB scheme in the GCM simulation. In addition, the "warm bias" in surface temperature over the high-latitude continental area in the GCM simulation (cf. section 3 in Part II) may also be attributed to larger evaporation than the observed. Further details on energy and water balance changes in the cold regions of the continent will be discussed in Part II.

5. Discussions and summary

A series of AGCM simulations were conducted to evaluate the relative roles of large-scale orography (i.e.,

TABLE 2. Surface energy budget for different regions. Averages are taken over the rainy season for each region: MC (annual), SA [Jun–Sep (JJAS)], EA (JJAS), Am (annual), WA [Jul–Sep (JAS)], and Sb [Jun–Aug (JJA)]; *R*, LE, and *H* denote net radiation and latent and sensible heat flux, respectively, in W m^{-2}. Net upward flux is shown as a positive value.

	MVS			MS			MR			NMR		
	R	LE	*H*	*R*	LE	*H*	*R*	LE	*H*	*R*	LE	*H*
MC	−148	116	31	−118	101	16	−109	68	41	−114	64	50
SA	−146	121	26	−123	109	15	−119	92	28	−114	70	44
EA	−146	117	22	−119	98	15	−108	63	38	−102	45	53
Am	−148	96	52	−112	67	44	−103	42	60	−104	46	57
WA	−137	98	41	−118	83	38	−117	72	46	−121	87	34
Sb	−135	96	23	−101	71	13	−98	41	37	−98	41	40

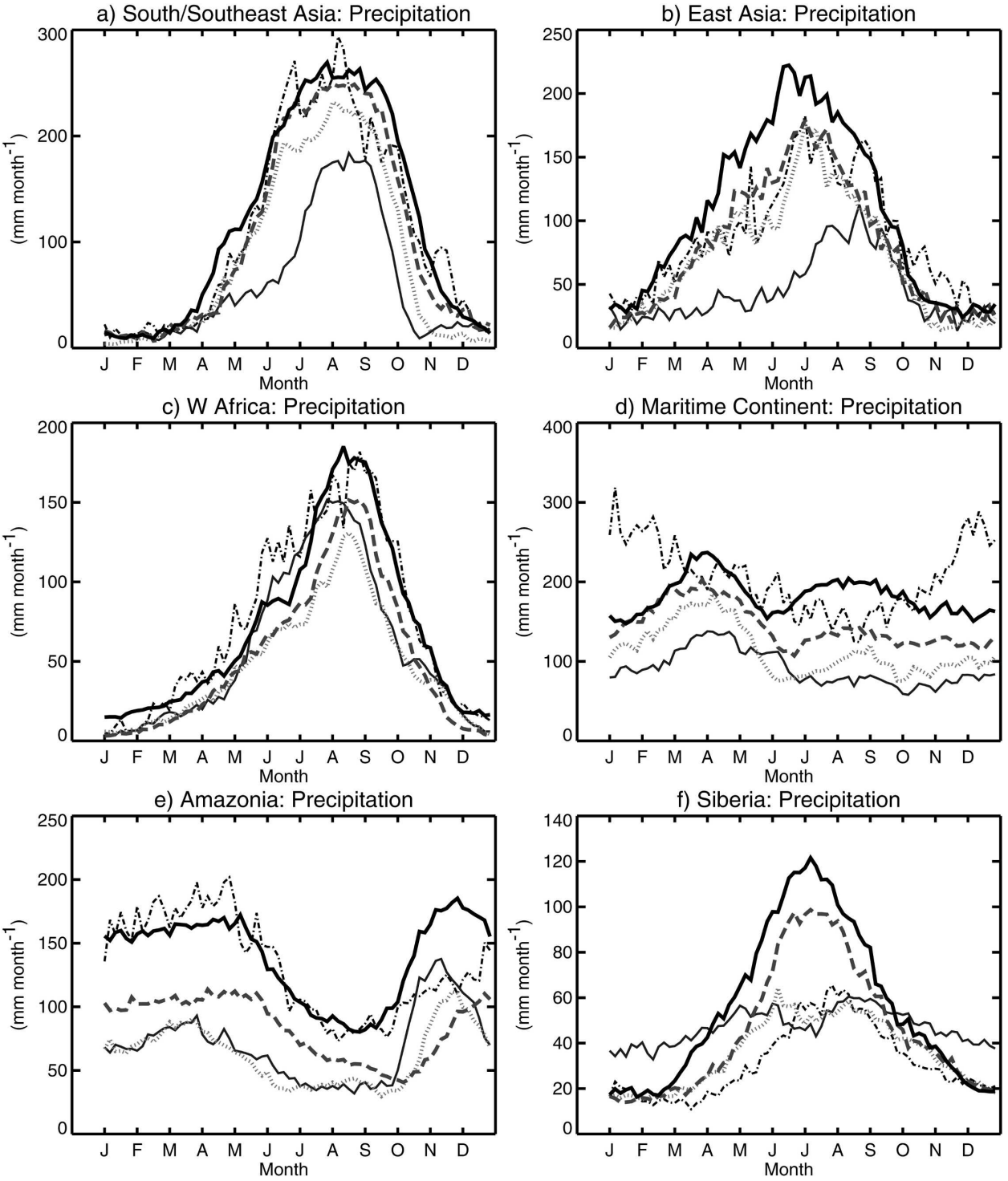

FIG. 10. Seasonal changes in precipitation for different regions from January to December. Thick solid, dashed, dotted, and thin lines denote MVS, MS, MR, and NMR runs, respectively. Thin dashed–dotted line is observation from CMAP.

the Tibetan Plateau) and land surface processes (represented by vegetation albedo/roughness and soil layer) on the hydroclimate of monsoon regions and the Tropics. Oceanic influences were set to be similar in each run, by using the monthly climatological SSTs in each run.

Hemispheric hydroclimate and circulations, and regional-scale energy and water balance, were compared

TABLE 3. Atmospheric water budget for different regions. Averages are for the same period as in Table 2 for each region; *C*, *E*, and *P* denote convergence, precipitation, and evaporation, respectively, in mm month^{-1}.

	MVS			MS			MR			NMR		
	C	*E*	*P*	*C*	*E*	*P*	*C*	*E*	*P*	*C*	*E*	*P*
MC	62	121	182	39	105	145	43	70	114	25	66	91
SA	115	125	241	112	113	225	100	95	196	60	72	133
EA	51	121	172	32	101	133	55	66	120	29	46	76
Am	40	99	139	14	70	84	19	44	63	22	48	70
WA	51	102	152	35	86	121	24	74	98	34	90	125
Sb	5	100	105	14	74	88	12	43	54	10	42	53

in the numerical experiments with the following four land surface conditions: a flat bare-rock surface (NMR), a bare-rock surface with orography (MR), a desert surface with soil and orography (MS), and a surface with realistic albedo/roughness with soil and orography (MVS). Major results are summarized as follows:

1) In the NMR run, the spatial distribution of precipitation during the northern summer monsoon was basically characterized by the ITCZ with a maximum over the warm western North Pacific (Fig. 3a). In the MR run (Fig. 3b), a more monsoonal pattern appeared, with maxima over the Bay of Bengal, along the southern and eastern slope of TP, and over eastern Asia. Precipitation over the warm western Pacific decreased compared to the NMR run (Fig. 4a). The overall spatial pattern of precipitation was similar to the current climate, but the amounts of precipitation in the monsoon region were about 60%–80% smaller than those in the MVS run and observations. Adding the albedo and roughness associated with the vegetation in the MVS run (Fig. 3c) further increased precipitation, particularly south and east of the TP, over the whole tropical land areas, and over boreal forests in northern Eurasia. Simultaneously, precipitation decreased further over the warm northwestern Pacific (Fig. 4b).
2) The TP generally enhanced components of the Asian monsoon circulation, deepening the monsoon trough over India (Fig. 5b) and the Tibetan high in the upper troposphere, with the northwest shift of the center position (Fig. 7b). These changes in the circulation (Figs. 6a and 8a) were basically interpreted as a stationary Rossby wave response to localized monsoonal heating over Asia (Rodwell and Hoskins 1996). In contrast, adding a vegetated surface with soil layer to Eurasia (the MVS run) resulted in a more selective enhancement of the subtropical anticyclone over the North Pacific and the northeastward extension of the Tibetan high in the upper troposphere (Figs. 6b and 8b). A continental vegetated surface is, therefore, more likely responsible for the large-scale heating contrast between the continents and the oceans, which may be a primary factor for formation of a subtropical anticyclone over the oceans (e.g., Rodwell and Hoskins 2001; Abe et al. 2004).
3) Regionally, the effects of TP on water budgets, as deduced by comparing the MR and NMR runs (Table 3), resulted in enhancement of precipitation in the Asian monsoon region (SA and EA), and reduction of precipitation in the West African monsoon region (WA). Enhanced downward motion over western Africa was associated with an enhanced large-scale, east–west circulation induced by TP orography, as noted by the previous GCM experiments (e.g., Broccoli and Manabe 1992; Rodwell and Hoskins 1996). Also, TP increased precipitation in the Maritime Continent, by enhancing convergence. Basically TP effect was very small in the water budget of northern Eurasia.
4) The sole effects of soil layer (inclusion of FC with 20 cm), as deduced from differences between the MS and MR runs (Table 3), appeared to be the increase of precipitation in all the regions from the Tropics to high latitudes. The increase of precipitation was primarily attributed to increase of evaporation, except for the tropical monsoon regions (SA and WA) where convergence also increased to some extent. The increase of FC has two effects: the surface temperature decreases because of an increase in heat capacity in the near-surface layer, and evaporation increases as available soil moisture increases. The net effect of increased FC is to increase net radiation and to increase evaporation (decrease the Bowen ratio, ratio of sensible heat flux to latent heat flux) as shown in Table 2. The decrease of surface temperature may tend to stabilize the atmosphere and reduce convergence in most of the regions.
5) The effects of vegetated surface (with albedo and roughness) are deduced by comparing the MVS and MS runs. A fundamental component of this effect is to increase available radiation as seen in the in-

crease of R (Table 2), and increase of E (under the large FC of the MVS run), which in turn increases precipitation (Table 3). It is interesting to note that in most of the regions in the Tropics and midlatitudes where available solar energy are large enough (as suggested from R in Table 2), both convergence and evaporation increase, and as a result, precipitation increases considerably. This positive feedback between evaporation and convergence (Dirmeyer and Shukla 1996; Zeng 1998) is likely to occur easily when and where radiative energy is sufficient and vegetation change is significant. This may imply that Charney's original hypothesis (Charney 1975; Charney et al. 1977) that the albedo significantly changes circulation and precipitation may be valid or effective only under this condition. In higher latitudes like Siberia (Sb), the increase of available energy solely increases evaporation, which is a primary source of precipitation there.

6) It may be worthwhile to roughly examine the relative impact of land surface processes (MVS run minus MR run) and that of TP topography (MR run minus NMR run). Note that the comparison is only preliminary and marginal, for the full evaluation may need to consider the nonlinearity and several feedbacks in the climate system. We presume that, as compared to the TP orography effect (TE), the surface vegetation (vegetation albedo and roughness) and soil layer (large FC) together should constitute a combined effect [land surface process effect (LSE)], since in reality vegetation and soil form an integrated surface system on land as mentioned in the introduction. Thus, the differences in precipitation between the MVS run and MR run, and those between the MR run and the NMR run could be a proxy measure of the LSE and TE, respectively.

In the Asian monsoon region (SA and EA), both LSE and TE values are around 50 (mm month^{-1}), suggesting that both land surface processes and TP contribute nearly equally to increase precipitation in this region. In MC and Am, LSE ($\sim$70) far exceeds TE ($\sim$0 to 20), suggesting LSE is more fundamental in the tropical rain forest regions. In Amazonia, the TE of the Andes, in fact, may play an additional role for precipitation, though this effect is implicitly included in the experiments here. In WA, LSE ($=$54) is as large as in the Asian monsoon region, though TE ($=-27$) considerably decreases precipitation. In Sb, precipitation in summer is basically attributed to LSE ($=$51), where TE is negligible but TE substantially induces large seasonal cycle with precipitation maximum in summer. Further description and discussion on changes in hydrology and hydroclimate in high latitudes will be made in Part II.

In this study, the present-day climatological SSTs were used, and because of warm oceans around the continents about a half of observed precipitation fell over most of the tropical and subtropical land regions even without TP and vegetation. However, some recent studies (e.g., Kitoh 2002; Abe et al. 2004) using coupled atmosphere–ocean (AO) GCMs have shown that the changes in land surface conditions, such as TP orography, change global SST distribution through radiative, thermodynamic, and dynamic feedbacks between land, atmosphere, and oceans (e.g., Kitoh 2002; Abe et al. 2004). Abe et al. (2004), for example, showed that without TP the warm water pool in the western Pacific (and the Maritime Continent) could not be formed. It could be, therefore, that weaker heating conditions in simulations with no TP and/or less vegetation may further suppress precipitation over land by cooling the warm pool region.

Another issue that warrants further study will be an evaluation with more realistic vegetation schemes, including stomatal control of transpiration. Over the tropical rain forest areas (MC and Am), for example, the simulated precipitation shows some systematic errors in the seasonal cycle of precipitation compared with observations (Figs. 10d and 10e). Over Sb, the amount of precipitation in summer season in the MVS run (Fig. 10f) is too large compared to the observed amount. Such discrepancies between the model results and observations may, at least partly, be related to systematic errors in the simple surface soil/vegetation scheme used here that does not allow realistic physiological control of energy and water budgets of the surface. Sophisticated vegetation biophysical schemes [e.g., SiB, biosphere–atmosphere transfer scheme (BATS), etc.] will provide skillful evaluation on the detailed variations of evapotranspiration [e.g., its components (transpiration/interception evaporation/ground surface evaporation), differences with vegetation types, short-term variations] with the photosynthetic processes, the canopy effects, and the multilayer treatment of soil moisture.

These remaining issues suggest that we pursue further investigation using a coupled AOGCM that incorporates a more sophisticated biosphere scheme, to evaluate the integrated effects of large-scale orography and full vegetation effects.

Acknowledgments. The authors would like to thank the anonymous reviewers for constructive suggestions and comments.

REFERENCES

Abe, M., A. Kitoh, and T. Yasunari, 2003: An evolution of the Asian summer monsoon associated with mountain uplift—Simulation with the MRI atmosphere–ocean coupled GCM. *J. Meteor. Soc. Japan,* **81,** 909–933.

——, T. Yasunari, and A. Kitoh, 2004: Effects of large-scale orography on the coupled atmosphere–ocean system in the tropical Indian and Pacific oceans in boreal summer. *J. Meteor. Soc. Japan,* **82,** 745–759.

Arakawa, A., and W. H. Schubert, 1974: Interaction of a cumulus cloud ensemble with the large-scale environment, Part I. *J. Atmos. Sci.,* **31,** 674–701.

——, and M. Suarez, 1983: Vertical differencing of the primitive equations in sigma coordinates. *Mon. Wea. Rev.,* **111,** 34–45.

Broccoli, A. J., and S. Manabe, 1992: The effects of orography on midlatitude Northern Hemisphere dry climate. *J. Climate,* **5,** 1181–1201.

Buol, S. W., F. D. Hole, and R. J. McCracken, 1997: *Soil Genesis and Classification*. 4th ed. Iowa State University Press, 527 pp.

Charney, J. G., 1975: Dynamics of deserts and drought in the Sahel. *Quart. J. Roy. Meteor. Soc.,* **101,** 193–202.

——, W. J. Quirk, S.-H. Chow, and J. Kornfied, 1977: A comparative study of the effects of albedo change on drought in semiarid regions. *J. Atmos. Sci.,* **34,** 1366–1385.

Dirmeyer, P. A., and J. Shukla, 1996: The effect on regional and global climate of expansion of the world's deserts. *Quart. J. Roy. Meteor. Soc.,* **122,** 451–482.

Gates, W. L., 1992: AMIP: The Atmospheric Model Intercomparison Project. *Bull. Amer. Meteor. Soc.,* **73,** 1962–1970.

Hahn, D. G., and S. Manabe, 1975: The role of mountains in the South Asian monsoon circulation. *J. Atmos. Sci.,* **32,** 1515–1541.

Haltiner, G. J., and R. T. Williams, 1980: *Numerical Prediction and Dynamic Meteorology.* Wiley, 477 pp.

Jenny, H., 1941: *Factors of Soil Formation; A System of Quantitative Pedology*. Dover Publications, 281 pp.

Kanae, S., Y. Hirabayashi, T. Yamada, and T. Oki, 2006: Influence of "realistic" land surface wetness on predictability of seasonal precipitation in boreal summer. *J. Climate,* **19,** 1450–1460.

Kitoh, A., 2002: Effect of large-scale mountains on surface climate—A coupled ocean–atmosphere general circulation. *J. Meteor. Soc. Japan,* **80,** 1165–1181.

Kondo, J., 1994: *Meteorology of Water Environment—Water and Energy Balances at the Earth Surface* (in Japanese). Asakura Shoten, 348 pp.

Le Treut, H., and Z.-X. Li, 1991: Sensitivity of an atmospheric general circulation model to prescribed SST changes: Feedback effects associated with the simulation of cloud optical properties. *Climate Dyn.,* **5,** 175–187.

Manabe, S., and T. B. Terpstra, 1974: The effects of mountains on the general circulation of the atmosphere as identified by numerical experiments. *J. Atmos. Sci.,* **31,** 3–42.

——, J. Smagorinski, and R. F. Strickler, 1965: Simulated climatology of a general circulation model with a hydrologic cycle. *Mon. Wea. Rev.,* **93,** 769–798.

Matthews, E., 1983: Global vegetation and land use: New high-resolution data bases for climate studies. *J. Climate Appl. Meteor.,* **22,** 474–487.

McFarlane, N. A., 1987: The effect of orographically excited gravity wave drag on the circulation of the lower stratosphere and troposphere. *J. Atmos. Sci.,* **44,** 1775–1800.

Mellor, G. L., and T. Yamada, 1974: A hierarchy of turbulence closure models for planetary boundary layers. *J. Atmos. Sci.,* **31,** 1791–1806.

Milly, P. C. D., and K. A. Dunne, 1994: Sensitivity of the global water cycle to the water-holding capacity of land. *J. Climate,* **7,** 506–526.

Moorthi, S., and M. J. Suarez, 1992: Relaxed Arakawa–Schubert: A parameterization of moist convection for general circulation models. *Mon. Wea. Rev.,* **120,** 978–1002.

Nakajima, T., M. Tsukamoto, Y. Tsushima, A. Numaguti, and T. Kimura, 2000: Modeling of the radiative process in an atmospheric general circulation model. *Appl. Opt.,* **39,** 4869–4878.

Nigam, S., I. M. Held, and S. W. Lyons, 1986: Linear simulation of stationary eddies in a general circulation model. Part I: The no-mountain model. *J. Atmos. Sci.,* **43,** 2944–2961.

——, ——, and ——, 1988: Linear simulation of stationary eddies in a general circulation model. Part II: The mountain model. *J. Atmos. Sci.,* **45,** 1433–1452.

Numaguti, A., 1999: Origin and recycling processes of precipitating water over the Eurasian continent: Experiments using an atmospheric general circulation model. *J. Geophys. Res.,* **104** (D2), 1957–1972.

Rodwell, M. J., and B. J. Hoskins, 1996: Monsoons and the dynamics of deserts. *Quart. J. Roy. Meteor. Soc.,* **122,** 1385–1404.

——, and ——, 2001: Subtropical anticyclones and summer monsoons. *J. Climate,* **14,** 3192–3211.

Saito, K., T. Yasunari, and K. Takata, 2006: Relative roles of large-scale orography and land surface processes in the global hydroclimate. Part II: Impacts on hydroclimate over Eurasia. *J. Hydrometeor.,* **7,** 642–659.

Sato, N., P. J. Sellers, D. A. Randall, E. K. Schneider, J. Shukla, J. L. Kinter III, Y.-T. Hou, and E. Albertazzi, 1989: Implementing the simple biosphere model in a general circulation model. *J. Atmos. Sci.,* **46,** 2757–2782.

Sellers, P. J., D. A. Randall, G. J. Collatz, and L. Bounoua, 1996: A revised land surface parameterization (SiB2) for atmospheric GCMs. Part I: Model formulation. *J. Climate,* **9,** 676–705.

Xie, P., and P. A. Arkin, 1997: Global precipitation: A 17-year monthly analysis based on gauge observation, satellite estimates, and numerical model outputs. *Bull. Amer. Meteor. Soc.,* **78,** 2539–2558.

Xue, Y., H.-M. H. Juang, W.-P. Li, S. Prince, R. DeFries, Y. Jiao, and R. Vasic, 2004: Role of land surface processes in monsoon development: East Asia and West Africa. *J. Geophys. Res.,* **109,** D03105, doi:10.1029/2003JD003556.

Zeng, N., 1998: Understanding climate sensitivity to tropical deforestation in a mechanistic model. *J. Climate,* **11,** 1969–1975.